

skii, who did much to facilitate the completion of this work.

<sup>1</sup>V. L. Berezinskii, *Nizkotemperaturnye svoïstva dvykhmer-nykh sistem s nepreryvnoi gruppoi simmetrii (Low-temperature Properties of Two-dimensional Systems with a Continuous Symmetry Group) (Dissertation).*

<sup>2</sup>V. L. Berezinskii and A. Ya. Blank, *Zh. Eksp. Teor. Fiz.* **64**, 725 (1973) [*Sov. Phys. JETP* **37**, 369 (1973)].

<sup>3</sup>A. M. Polyakov, *Phys. Lett.* **59B**, 79 (1975).

<sup>4</sup>A. A. Migdal, *Zh. Eksp. Teor. Fiz.* **69**, 1457 (1975) [*Sov. Phys. JETP* **42**, 743 (1975)].

<sup>5</sup>L. J. de Jongh, W. D. Van Amstel and A. R. Miedema, *Physica* **58**, 277 (1972).

<sup>6</sup>D. Ruelle, *Statistical Mechanics—Rigorous Results*, Benjamin, N. Y., 1969 (Russ. transl., Mir, M., 1971).

<sup>7</sup>V. L. Pokrovskii and G. V. Uimin, *Zh. Eksp. Teor. Fiz.* **65**, 1691 (1973) [*Sov. Phys. JETP* **38**, 847 (1974)].

Translated by P. J. Shephard

## Influence of pressure on the Fermi surface of cadmium

V. A. Venttsel', O. A. Voronov, A. I. Likhter, and A. V. Rudnev

*Institute of High-Pressure Physics, USSR Academy of Sciences, Moscow*

(Submitted July 16, 1975)

*Zh. Eksp. Teor. Fiz.* **70**, 272–280 (January 1976)

Measurements were made of the areas of the extremal sections of the Fermi surface of cadmium and their pressure dependences were determined for magnetic field directions lying in the crystallographic planes (10 $\bar{1}$ 0) and (11 $\bar{2}$ 0). These experimental results were used in a calculation—within the local pseudopotential model—of the matrix elements of the pseudopotential and their pressure derivatives.

PACS numbers: 71.30.Hr

1. The present paper reports an investigation of the Fermi surface of cadmium and the influence of hydrostatic pressure on this surface. Cadmium is characterized by a strong compressibility anisotropy, so that one can expect large changes under pressure. Investigations of the influence of pressure on the dimensions of the various parts of the Fermi surface make it possible to interpret more reliably the observed oscillation frequencies and to calculate, within the framework of the adopted model, the pressure dependences of the matrix elements of the pseudopotential. In these calculations use is made of the local pseudopotential model whose matrix elements  $W_q$  are governed only by the reciprocal lattice vectors  $q_i$  and are identical at all points in the Brillouin zone.

Like other hexagonal metals of the second group in the periodic table, cadmium has a Fermi surface which can be described qualitatively but satisfactorily by the model of almost-free electrons. This means that if we use the local pseudopotential approximation and the OPW method, we can calculate relatively simply and in a clear manner the areas of extremal sections of the Fermi surface and their pressure dependences, and to determine the matrix elements of the pseudopotential and their pressure dependences from a comparison of the calculated and experimental results. Such data can be used to explain the behavior of some macroscopic properties under pressure, such as the electrical resistivity, magnetoresistance, etc., and to estimate the pressure at which the topology of the Fermi surface changes. Investigations of the influence of pressure on the matrix elements of the pseudopotential are also important from the point of view of the pseudopotential theory because they can give information on the depen-

dence of the pseudopotential on the wave vector.

In the one-wave approximation the Fermi surface of cadmium is of the same form as the Fermi surfaces of other divalent hexagonal metals,<sup>[1]</sup> but the radius of the Fermi sphere of free electrons  $k_F$  is less than the side  $a$  of the hexagonal base of the prism and, consequently, there are no needles or electron surfaces in the third Brillouin zone (Fig. 1).

The lattice potential alters not only the dimensions but also the shape of the Fermi surface of cadmium: the horizontal arms of the monster in the second Brillouin zone are broken, and the butterfly in the third Brillouin zone as well as the cigar in the fourth zone are absent, as shown by calculations of Falicov and Stark.<sup>[2]</sup>

Thus, according to the model of Tsui and Stark<sup>[3]</sup> the Fermi surface of cadmium consists of two hole pockets ( $\alpha$ ) in the first Brillouin zone and of the residue of the monster in the second Brillouin zone, and also of one electron lens ( $\beta$ ) at the center of the third zone. In the extended-zone scheme the monster is a corrugated cylinder elongated along the [0001] axis and it has a minimal section  $\beta$  in the  $ALH$  plane in the region of the point  $H$  in the Brillouin zone. The section  $\beta$  includes the pocket  $\alpha$  and it is separated from it by the spin-orbit gap. The maximum section of the monster  $\gamma$  in the plane  $\Gamma MK$  of the Brillouin zone is formed by residues of three monsters in contact and it consists of three sheets. As shown in Refs. 3 and 4, magnetic breakdown in various fields gives either the total cross section  $S_\gamma$  (in strong and weak fields) or  $\frac{1}{3}S_\gamma$  and  $\frac{2}{3}S_\gamma$  (in the range of intermediate magnetic fields). In addition to the frequencies of the oscillations corresponding to these sections, other

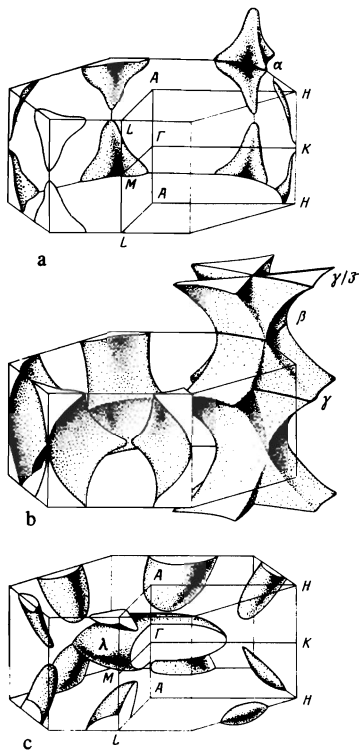


FIG. 1. Model of the Fermi surface of cadmium: a) first Brillouin zone; b) second Brillouin zone; c) third Brillouin zone; the right-hand lower corner shows the cigar located in the fourth Brillouin zone.

oscillations are reported in<sup>[3,4]</sup> but they have not yet been interpreted reliably.

2. An investigation of the Fermi surface of cadmium and of the influence of pressure on the surface was made by measuring the de Haas-van Alphen effect using apparatus described earlier.<sup>[5]</sup> Measurements of the hf oscillations were made in a superconducting solenoid (producing fields up to 55 kOe) in the short-circuited state and records were obtained at the 12-th harmonic of the modulation frequency. In hf oscillation measurements we usually recorded the second harmonic. In those cases when it was desirable to carry out measurements in stronger fields, we used apparatus producing pulse magnetic fields (up to 100 kOe). Measurements of the angular dependences of the oscillation frequencies and their pressure dependences were carried out on samples of  $0.8 \times 1 \times 10$  mm dimensions cut by spark machining from a bulk single crystal. Samples were oriented along the three principal crystallographic planes (0001),  $(10\bar{1}0)$  and  $(11\bar{2}0)$  in steps of  $10^\circ$  and the orientation of each sample was additionally determined by x-ray diffraction.

In pulsed magnetic fields in the absence of pressure the angular dependences were obtained by rotating a sample relative to the direction of H,<sup>[6]</sup> whereas under pressure we used a system with two samples of the same orientation located in two parallel stainless-steel tubes (3 mm in diameter); in one of them we applied a hydrostatic pressure transmitted by liquid helium and in the other only the helium bath pressure was maintained. Oscillations due to the two samples in the

absence of pressure were displayed on the screen of a double-beam oscillograph and then a study was made of the oscillations produced when one of the samples was subjected to pressure. We measured the phase shift of the oscillations of one sample relative to the other which was under pressure and, as in the case of a static field, we found the frequency from the formula

$$\frac{1}{F} \frac{\Delta F}{\Delta p} = \frac{1}{2\pi} \frac{\Delta \psi}{\Delta p} \frac{H}{F}.$$

The reliability of the results was improved by raising the pressure several times and determining the average phase shift  $\Delta\psi$ . A detailed description of the various parts of the apparatus used in measurements under pressure in pulse fields will be given in a separate communication.

3. The frequencies of the oscillations in the  $(10\bar{1}0)$  and  $(11\bar{2}0)$  planes were in good agreement with the results reported in<sup>[3,4]</sup>, but they were observed in a somewhat different range, as discussed in detail later. The curves in Fig. 2 are plotted on the basis of the results of Tsui and Stark<sup>[3,4]</sup> but for the sake of clarity we included in Fig. 2 (black dots) only those values of the frequencies which we determined in pulse fields and which were not given in<sup>[3,4]</sup>. We used open circles in Fig. 2 to denote that the pressure dependence of a section was determined in a given orientation. The angular dependences of the pressure coefficient  $d(\ln S)/dp = f(\varphi)$  are plotted for several sections in Fig. 2.

Oscillations of frequency  $\alpha$ , corresponding to sections through pockets in the first Brillouin zone (Fig. 1a), were observed throughout the investigated angular range and the area of the section agreed with the published data.<sup>[4]</sup> This area decreased under pressure but the pressure coefficient remained practically constant up to angles of  $\sim 70^\circ$  (Fig. 3) and then it reached the value  $(-13.5 \pm 0.5) \times 10^{-3} \text{ kbar}^{-1}$  for H  $\parallel [11\bar{2}0]$  and  $(-15.4 \pm 1) \times 10^{-3} \text{ kbar}^{-1}$  for H  $\parallel [10\bar{1}0]$ . The frequency  $2\alpha$  could be regarded as the second harmonic of the oscillation frequency  $\alpha$ , which was deduced from the

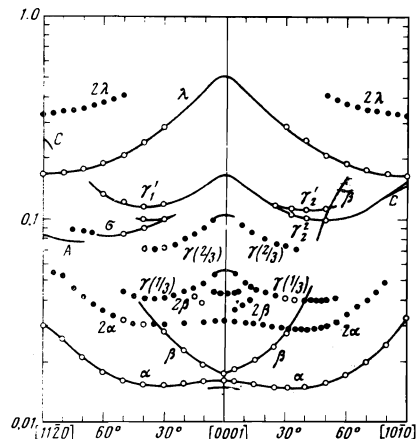


FIG. 2. Dependences of the areas of extremal sections (in atomic units) on the orientation. The continuous curves are based on the results in<sup>[3,4]</sup>, the open circles represent the cross sections measured under pressure, and the black dots the measurements in pulse magnetic fields.

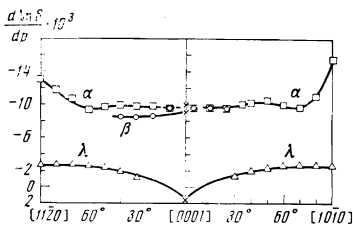


FIG. 3. Angular dependences of  $d[\ln S(\varphi)]/dp$ ; the crosses represent the results taken from<sup>[7]</sup>.

ratios of the frequencies throughout the investigated angular range, ratio of the effective masses (in the range  $\varphi = 20^\circ - 30^\circ$ ,  $m/m_0$  was 0.14–0.15 for the  $\alpha$  oscillations and 0.27–0.29 for  $2\alpha$ ), and constant value of the pressure coefficient. The section  $\beta$  also decreased under pressure and the pressure coefficient was  $(-9.1 \pm 0.5) \times 10^{-3} \text{ kbar}^{-1}$  for  $H \parallel [0001]$ ; it remained practically constant for angles deviating from this axis by  $40^\circ$  in the  $(10\bar{1}0)$  plane (Fig. 3). When  $H$  was directed along the  $[0001]$  axis or when it made angles up to  $15^\circ$  with this axis, we again observed the doubled oscillation frequency  $2\beta$ .

Three groups of oscillations were observed above  $\alpha$  and  $\beta$ : these groups are usually identified with the section  $\gamma$  of the monster<sup>[3,4]</sup> and represent either a section of the whole three-section surface  $S_\gamma$  or of one ( $\frac{1}{3}S_\gamma$ ) or two ( $\frac{2}{3}S_\gamma$ ) of its sheets (Fig. 1b). The section  $\gamma$  was obtained in<sup>[3,4]</sup> in a wide range of angles  $0 < \varphi < 70^\circ$  in the  $(10\bar{1}0)$  plane and  $0 < \varphi < 55^\circ$  in the  $(11\bar{2}0)$  plane, whereas the sections  $\frac{1}{3}S_\gamma$  and  $\frac{2}{3}S_\gamma$  were found within an interval of  $\sim 5^\circ$  near the  $[0001]$  axis. We observed the sections  $\gamma$  within the range  $10^\circ < \varphi < 70^\circ$  in the plane  $(10\bar{1}0)$  and for  $10^\circ < \varphi < 55^\circ$  in the plane  $(11\bar{2}0)$ ; for angles  $\varphi < 10^\circ$ , the oscillation amplitude fell steeply. We were able to measure reliably the change in this section under pressure in a narrower range of angles  $30^\circ < \varphi < 60^\circ$  in the  $(10\bar{1}0)$  plane and in  $25^\circ < \varphi < 50^\circ$  in the  $(11\bar{2}0)$  plane. The sections  $\frac{1}{3}S_\gamma$  and  $\frac{2}{3}S_\gamma$  were obtained by us over a wide range of angles in both planes: the oscillations corresponding to  $\frac{1}{3}\gamma$  were visible up to  $55^\circ$  and those corresponding to the  $\frac{2}{3}\gamma$ —up to  $40^\circ$  (Fig. 2). The frequency  $\gamma$  decreased under pressure at a rate  $(-1.5 \pm 0.2) \times 10^{-3} \text{ kbar}^{-1}$  for angles  $30^\circ < \varphi < 60^\circ$  in the plane  $(10\bar{1}0)$  and for  $30^\circ < \varphi < 40^\circ$  in the plane  $(11\bar{2}0)$ . The measurement error increased in the range  $\varphi < 30^\circ$  but it was clear from our results and those in<sup>[8]</sup> that one could expect a change in the sign of the derivative  $d(\ln S_\gamma)/dp$  in the range  $15^\circ < \varphi < 20^\circ$ . The branch  $\gamma$  in the  $(11\bar{2}0)$  plane was split into two for angles  $\varphi > 25^\circ$ : These branches were  $\gamma_2^2$  and  $\gamma_2^1$ <sup>[3,4]</sup> (Fig. 2). Under pressure the frequency  $\gamma_2^1$  decreased more rapidly than  $\gamma_2^2$  and at  $\varphi \approx 40^\circ$  this reduction was

$$d[\ln S(\gamma_2^1)]/dp = (-3.6 \pm 0.5) \cdot 10^{-3} \text{ kbar}^{-1}.$$

The changes under pressure of the sections  $\frac{1}{3}\gamma$  and  $\frac{2}{3}\gamma$  could not be recorded reliably. For example, for  $\varphi \approx 20^\circ$  in both planes we found that

$$d[\ln S(\frac{1}{3}\gamma)]/dp = (0 \pm 1) \cdot 10^{-3} \text{ kbar}^{-1}.$$

There was no doubt about the interpretation of the

oscillation frequency  $\lambda$  associated with the lens section in the third Brillouin zone (Fig. 1c). Such oscillations, corresponding to the second harmonic of this frequency, were observed near the  $[10\bar{1}0]$  and  $[11\bar{2}0]$  axes. Under pressure this lens section decreased at a rate  $d(\ln S)/dp$  which changed from  $(-2.8 \pm 0.2) \times 10^{-3} \text{ kbar}^{-1}$  in fields  $H \perp [0001]$  to  $(-1.2 \pm 0.2) \times 10^{-3} \text{ kbar}^{-1}$  for  $\varphi = 30^\circ$  (Fig. 3). The pressure dependence of the maximal section of the lens were determined in<sup>[7]</sup> and it was found that it increased at a rate of  $+1.6 \times 10^{-3} \text{ kbar}^{-1}$ . This indicated flattening of the lens accompanied by a simultaneous increase of its diameter. We used the calculated values of the pseudopotential form factors and their pressure dependences (Table 2) in a computer calculation of the orientational dependence of  $d(\ln S_\gamma)/dp$ . The continuous curve in Fig. 3 for the  $\lambda$  oscillations is based on these calculations. We can see from Fig. 3 that the calculated curve is in good agreement with the experimental points.

Other oscillations could not be identified reliably with any specific Fermi surface sections. In a narrow range of angles near the hexagonal axis ( $\varphi \lesssim 10^\circ$ ) we observed beats of the frequencies  $\alpha$  and  $\chi$  ( $F = 5.4 \times 10^6 \text{ Oe}$ ), which were reported in<sup>[9,10]</sup>. Oscillations of frequency  $\sigma$  were observed in the angular range from  $30^\circ$  to  $75^\circ$  in the  $(10\bar{1}0)$  plane, and in the range  $30^\circ - 40^\circ$  the pressure coefficient of this frequency was  $(-2.8 \pm 0.5) \times 10^{-3} \text{ kbar}^{-1}$ .

4. We calculated the matrix elements of the pseudopotential and their pressure dependences by the OPW method with a local pseudopotential. The shape and dimensions of the Fermi surface were governed primarily by three matrix elements:  $W_{0002}$ ,  $W_{10\bar{1}0}$ , and  $W_{10\bar{1}1}$  (one element was  $W_{0001} = 0$  because the structure factor  $S_{0001}$  vanished), and also by the spin-orbit splitting  $\lambda$ . In these calculations we selected the following sections governed by the form factors (the matrix element  $W_i$  was a product of the structure factor  $S_i$  and the form factor  $w$ ): a) the lens ( $w_{0002}$ ) along the two directions  $H \perp (0001)$  and  $H \parallel (0001)$ ; b) the monster section  $\gamma$  ( $w_{0002}$ ,  $w_{10\bar{1}0}$ , and  $w_{10\bar{1}1}$ ) for  $H \perp (0001)$ ; c) the monster section  $\beta$  ( $w_{10\bar{1}0}$ ,  $w_{10\bar{1}1}$ , and  $\lambda$ ) for  $H \perp (0001)$ ; d) the section through the pockets  $\alpha$  ( $w_{10\bar{1}0}$ ,  $w_{10\bar{1}1}$ , and  $\lambda$ ) for  $H \perp (0001)$ ,  $H \perp (10\bar{1}0)$ , and  $H \perp (11\bar{2}0)$ . The calculations were carried out on a BÉSM-4 computer for two sets of the Brillouin zone parameters corresponding to  $p = 0$  and  $p = 1 \text{ kbar}$  (Table 1). The lens section was determined in the 2-OPW approximation. The use of a large number of plane waves altered the section area by not more than 0.1%. Therefore, in all these calculations we used the minimum number of plane waves

TABLE 1. Brillouin zone parameters and their pressure dependences.

Parameter*	$p=0$	$p=1 \text{ kbar}$	$\frac{1}{10^{-3}} \frac{dq}{dp} \text{ kbar}^{-1}$
$a$	0.746706	0.746892	0.249
$b$	0.601662	0.602494	1.383

\*The parameters were calculated on the basis of the results in<sup>[12,13]</sup>.

TABLE 2. Values of  $w_q$ ,  $\lambda$ , and  $\epsilon_F$  and their pressure dependences.

$q$	$w_q$ , at. units ( $W_q = Sw_q$ )				$\frac{dw}{dp} \cdot 10^4$ at. units/kbar	
	Our results	[14]	[15]	[16]	Our results	[7]
[0002]	-0.0261	-0.025	-0.026	-0.018	-2.8	-3.4
[1010]	-0.00173	-0.0050	-0.0060	+0.0040	+2.0	-
[1011]	+0.0120	+0.014	+0.014	+0.018	-0.4	-
$\lambda$	0.00706	-	-	0.0065	-0.08	-
$\epsilon_F$	0.280	0.279	0.279	0.276	-	-

needed to ensure that the calculated and experimental section areas agreed within 5–10%. In calculating the area of the section  $\frac{1}{3}\gamma$  it was sufficient to use five plane waves, for the area of the section of the pockets by the (1010) and (1120) planes we needed six plane waves, and for the areas of the sections  $\alpha$  and  $\beta$  formed by the (0001) plane we had to allow for the spin-orbit interaction and this doubled the matrix rank.

The procedure used in the calculation of the form factors reduced to the derivation of the secular equation for the wave vectors  $\mathbf{k}$  located near a certain symmetry point  $k_0$ , including all the reciprocal lattice vectors  $\mathbf{q}_i$  governing a given section of the Fermi surface. The lattice parameters governed the values of the vectors  $\mathbf{q}_i$  and the Fermi energy because in the one-wave approximation the value of  $\epsilon_F = k_F^2/2$  was determined only by the Brillouin zone volume. Secular equations of this kind were solved for  $k$ , the section areas  $S_{\text{calc}}$  were calculated for various values of  $w_i$ , these areas were compared with the experimental values  $S_{\text{exp}}$ , and hence the form factors  $w_i$  were determined. The optimal set of values of  $w_i$  and  $\lambda$  was found by the least-squares method, i.e., we determined the minimum of the sum

$$\sum_{i=1}^n \left( \frac{S_{\text{exp}} - S_{\text{calc}}^{(i)}}{S_{\text{exp}}^{(i)}} \right)^2$$

assuming also that: a) the arms of the monster were

broken and b) there was no needle at the point  $K$  in the third Brillouin zone.

In the initial calculations it was assumed that  $\epsilon_F = k_F^2/2$  was governed only by the Brillouin zone volume. In minimization the value of  $\epsilon_F$  was used as an adjustable parameter since otherwise it was not possible to achieve agreement between  $S_{\text{exp}}$  and  $S_{\text{calc}}$  better than 30% but by varying  $\epsilon_F$  within a narrow range (less than 0.25%) it was possible to match  $S_{\text{calc}}$  and  $S_{\text{exp}}$  within 10%. The signs of the form factors  $w_{0002}$  and  $w_{0011}$  were selected on the basis of the generally accepted form of the dependence  $w(q)$  and the sign of  $w_{1010}$  was found to be negative by a minimization procedure. The calculated values of  $w_i$ ,  $\lambda$  and  $\epsilon_F$  are listed in the first column of Table 2 and the next three columns give the published values.<sup>[14–16]</sup> The spin-orbit interaction of a free atom was given in<sup>[17]</sup> and amounted to 0.005 at. units. The last two columns of Table 2 give the derivatives of the form factors calculated from the experimental data.

The values of  $w_i$  and  $dw_i/dp$  given in Table 2 were used in a calculation of the section areas  $S_{\text{calc}}$ , their derivatives  $[d(\ln S_i)/dp]_{\text{calc}}$ , and some linear dimensions of the Fermi surface. Table 3 gives the results of these calculations and compares them with the experimental data obtained in the present study and in<sup>[3,4,7,18]</sup>. It is clear from Table 3 that the agreement between the calculated and experimental values is in all cases within 10% but it must be stressed that the greatest discrepancies are observed for the dimensions of the maximum section of the lens and of the section  $\gamma$ . If we had used a larger number of plane waves, nonlocal pseudopotential, or other calculation methods such as the Green functions or the PPW method we could have naturally improved the agreement between  $S_{\text{exp}}$  and  $S_{\text{calc}}$  but we would have lost the simplicity and clarity which enabled us to calculate not only the form factors  $w_i$  but also their pressure dependences.

5. According to Arkhipov,<sup>[19]</sup> there should exist a universal representation of the pseudopotential suitable

TABLE 3. Comparison of calculated and measured dimensions of Fermi surface of cadmium.\*

Fermi surface section	$S_{\text{extr}}$ , at. units		$d(\ln S)/dp$ , $10^{-3}$ kbar $^{-1}$			Linear dimensions, at. units		
	E**	C	Our results	[7]	C	E <sup>[18]</sup>	C	k
Lens $\lambda$								
H $\perp$ (0001)	0.501	0.458	-	+1.6 $\pm$ 0.6	+1.61	0.413	0.382	(k $\perp$ [0001])
H $\parallel$ (0001)	0.165	0.157	-2.7 $\pm$ 0.5	-2.3 $\pm$ 0.3	-2.61	0.146	0.142	(k $\parallel$ [0001])
Pocket $\alpha$								
H $\perp$ (0001)	0.0159	0.0158	-9.7 $\pm$ 0.2	-9.7 $\pm$ 0.2	-9.44	-	-	-
H $\perp$ (1120)	0.0324	0.0328	-15.4 $\pm$ 1	-	-15.7	0.057	0.055	(k $\parallel$ [1120])
H $\perp$ (1010)	0.0294	0.0296	-13.5 $\pm$ 0.5	-13.2 $\pm$ 0.2	-13.8	0.094	0.093	(k $\parallel$ [1010])
Monster $\beta$								
H $\perp$ (0001)	0.0171	0.0170	-9.1 $\pm$ 0.5	-9.1 $\pm$ 0.5	-8.95	0.059	0.055	(k $\parallel$ [1120])
Monster $\gamma$								
H $\perp$ (0001)	0.163	0.174	-	+1.0 $\pm$ 0.5 [8]	-	0.261	0.247	(k $\parallel$ [1010])
Monster $\gamma_2^1$								
40 $^\circ$ in the (1120) plane	0.113	-	-3.6 $\pm$ 0.5	-	-	-	-	-
Monster $\gamma_2^2$								
40 $^\circ$ in the (1120) plane	0.102	-	-1.1 $\pm$ 0.5	-	-	-	-	-
Monster $\gamma_1^1$								
40 $^\circ$ in the (1010) plane	0.115	-	-1.1 $\pm$ 0.5	-	-	-	-	-
Monster $\frac{1}{2}\gamma$								
30 $^\circ$ in the (1120) plane	0.041	-	0.0 $\pm$ 1.0	-	-	-	-	-
Monster $\sigma$								
40 $^\circ$ in the (1010) plane	0.090	-	-2.85 $\pm$ 0.5	-	-	-	-	-

\*E denotes experimental results and C the calculated ones.

\*\*The results of Tsui and Stark<sup>[3,4]</sup> and our values.

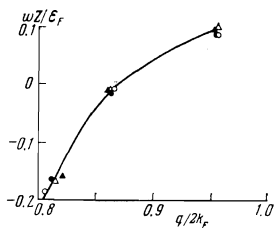


FIG. 4. Dependence of the pseudopotential on the wave vector:  $\Delta$ ,  $\blacktriangle$  zinc;<sup>[5]</sup>  $\circ$ ,  $\bullet$  cadmium in the representation used in<sup>[19]</sup>. The open circles correspond to  $p = 0$  and the black dots to  $p = 10$  kbar.

for all nontransition metals and, consequently, capable of describing the dependence of the pseudopotential on the lattice parameters. In this representation the dimensionless pseudopotential  $Zw/\epsilon_F$  is a function of the dimensionless wave vector  $q/2k_F$ . Figure 4 gives the dependence  $Zw/\epsilon_F = f(q/2k_F)$  for two hexagonal metals — zinc<sup>[5]</sup> and cadmium at pressures  $p = 0$  and (for clarity) at  $p = 10$  kbar. It is clear from Fig. 4 that all the points lie near the common curve and, consequently, the Arkhipov representation of the pseudopotential is a suitable method for the description of its behavior under pressure. The numerical values of  $Zw/\epsilon_F(q/2k_F)$  given in Fig. 4 differ from those in<sup>[19]</sup> but this is not of great importance because Arkhipov obtained his expressions from first principles and these expressions had no adjustable parameters.

The data presented in Table 2 could also be used to calculate the critical (transition) pressure  $p_c$  at which the arms of the monster came into contact and a needle appeared. When the arms of the monster joined, the appearance of a needle gave rise to singularities in the magnetoresistance recorded for  $H \parallel [0001]$  due to magnetic breakdown through the needle.<sup>[20]</sup> According to our calculations the monster arms should join at  $p_c < 10$  kbar and a needle should appear at  $p_c = 43 \pm 25$  kbar. The indeterminacy in the value of  $p_c$  was due to the sensitivity of  $p_c$  to  $dw_{10\bar{1}0}/dp$ , which was  $(2 \pm 0.2) \times 10^{-4}$  at. units/kbar and depended on the precision of the determination of  $d(\ln S_i)/dp$ . In<sup>[21]</sup> it was reported that the application of a pressure  $p = 15$  kbar produced a deep minimum in the angular dependence of the magnetoresistance recorded in a field  $H \parallel [0001]$  and this minimum was attributed to the appearance of a needle and joining of the monster arms. Our calculations of  $p_c$  agreed, within the limits of the experimental error, with the results in<sup>[21]</sup>.

Measurements of the electrical resistivity of a cadmium single crystal [ $J \parallel (0001)$ ] reported in<sup>[22]</sup> revealed a resistivity jump at  $p \approx 30$  kbar. These measurements were carried out at room temperature under natural hydrostatic conditions. This pressure could be compared with  $p_c$  bearing in mind the temperature dependences of the lattice parameters but we could assume qualitatively that the jump was due to the appearance of a needle.

The form factor values given in Table 2 were used in a calculation of the areas of extremal sections of the

Fermi surface near the point  $L$  in the third Brillouin zone. For the cigar this area in  $H \parallel [0001]$  was 0.0185 at. units, which was close to the frequency  $\chi$  mentioned above (Fig. 2). None of the oscillation frequencies obtained in our study could be identified with the butterfly cross section.

The authors regard it as their pleasant duty to thank L. F. Vereshchagin for his continuous interest in this investigation, R. G. Arkhipov, A. P. Kochkin, and E. S. Itskevich for valuable discussions.

<sup>1</sup>The frequency  $\chi$  was investigated in detail in<sup>[11]</sup> and attributed there to the cigar section in the fourth Brillouin zone.

- <sup>1</sup>W. A. Harrison, Phys. Rev. **118**, 1190 (1960).  
<sup>2</sup>R. W. Stark and L. M. Falicov, Phys. Rev. Lett. **19**, 795 (1967).  
<sup>3</sup>D. C. Tsui and R. W. Stark, Phys. Rev. Lett. **16**, 19 (1966).  
<sup>4</sup>D. C. Tsui and R. W. Stark, The de Haas-van Alphen Spectrum of Cadmium (Preprint).  
<sup>5</sup>V. A. Venttsel', O. A. Voronov, A. I. Likhter, and A. V. Rudnev, Zh. Eksp. Teor. Fiz. **65**, 2445 (1973) [Sov. Phys. -JETP **38**, 1220 (1974)].  
<sup>6</sup>V. A. Venttsel', A. I. Likhter, and A. V. Rudnev, Zh. Eksp. Teor. Fiz. **53**, 108 (1967) [Sov. Phys. -JETP **26**, 73 (1968)].  
<sup>7</sup>H. J. Bryant and J. J. Vuillemin, Phys. Rev. B **9**, 3193 (1974).  
<sup>8</sup>J. E. Schirber and W. J. O'Sullivan, Proc. Eleventh Intern. Conf. on Low Temperature Physics, St. Andrews University, Scotland, 1968, Vol. 2, publ. by St. Andrews University (1969), p. 1141.  
<sup>9</sup>A. D. C. Grassie, Philos. Mag. **9**, 847 (1964).  
<sup>10</sup>A. S. Joseph, W. L. Gordon, J. R. Reitz, and T. G. Eck, Phys. Rev. Lett. **7**, 334 (1961).  
<sup>11</sup>E. S. Itskevich, A. M. Sobko, V. A. Sykhoparov, and I. M. Templeton, Dokl. na V. Mezhdunar. konf. po fizike i tekhnike vysokikh davlenii (Paper presented at Fifth Intern. Conf. on Physics and Technology of High Pressures), M., 1975.  
<sup>12</sup>R. D. McCammon and G. K. White, Philos. Mag. **11**, 1125 (1965).  
<sup>13</sup>C. W. Garland and J. Silverman, Phys. Rev. **119**, 218 (1960).  
<sup>14</sup>S. Katsuki and M. Tsuji, J. Phys. Soc. Jpn. **20**, 1136 (1965).  
<sup>15</sup>A. A. Mar'yakhin and I. V. Svechkarov, Phys. Status Solidi **23**, K133 (1967).  
<sup>16</sup>A. A. Mar'yakhin and I. V. Svechkarov, Phys. Status Solidi **33**, K37 (1969).  
<sup>17</sup>M. H. Cohen and L. M. Falicov, Phys. Rev. Lett. **5**, 544 (1960).  
<sup>18</sup>R. C. Jones, R. G. Goodrich, and L. M. Falicov, Phys. Rev. **174**, 672 (1968).  
<sup>19</sup>R. G. Arkhipov, Zh. Eksp. Teor. Fiz. **59**, 1711 (1970) [Sov. Phys. -JETP **32**, 921 (1971)].  
<sup>20</sup>R. W. Stark and L. M. Falicov, Prog. Low Temp. Phys. **5**, 235 (1967).  
<sup>21</sup>E. S. Itskevich and A. N. Voronovskii, Pis'ma Zh. Eksp. Teor. Fiz. **4**, 226 (1966) [JETP Lett. **4**, 154 (1966)].  
<sup>22</sup>A. N. Ivanov, V. V. Kechin, A. I. Likhter, and E. M. Ogneva, Dokl. na V. Mezhdunar. konf. po fizike i tekhnike vysokikh davlenii (Paper presented at Fifth Intern. Conf. on Physics and Technology of High Pressures), M., 1975.

Translated by A. Tybulewicz